Structural, thermal, and spectral investigations of the lanthanide(III) biphenyl-4,4′-dicarboxylates

Justyna Sienkiewicz-Gromiuk · Zofia Rzączyńska

Abstract The lanthanide biphenyl-4,4′-dicarboxylates (bpdc) series of the general formulae $Ln_2(bpdc)_3 \cdot nH_2O$, where Ln = lanthanides from La(III) to Lu(III); bpdc = $C_{12}H_5(COO)_2^{2-}$; n = 4, 5 or 6 have been obtained by the conventional precipitation method. All prepared complexes were characterized by elemental analysis, simultaneous thermal analyses thermogravimetric-differential scanning calorimetry (TG–DSC) and TG–FT-IR, FT-IR, and FT-Raman spectroscopy as well as X-ray diffraction patterns measurements. In the whole series of analyzed complexes the $bpdc^{2-}$ ligand is completely deprotonated. In view of that, four carboxylate oxygen atoms are engaged in the coordination of Ln(III) ions. The synthesized compounds are polycrystalline and insoluble in water. They crystallize in the low symmetry crystal systems, like monoclinic and triclinic. Heating in the air atmosphere resulted in the multi-steps decomposition process, namely endothermic dehydration and strong exothermic decomposition processes. The dehydration process leads to the formation of stable anhydrous Ln_2bpdc_3 compounds which subsequently decompose to the corresponding lanthanide oxides.

Keywords Biphenyl-4,4′-dicarboxylic acid · Lanthanide complexes · TG–DSC · TG–FT-IR · FT-IR

Introduction

Synthesis of metal-based coordination polymers with novel structures constitutes an important area of research.

Coordination polymers (PCPs) represent a unique class of crystalline open framework solids with unprecedented structures and diverse chemical composition [1, 2]. These kinds of compounds result from molecular reactions between metal ions and bridging multidentate organic ligands, usually performed under hydro(solvo)thermal conditions [3]. The aromatic polycarboxylates are often employed in a design strategy to construct metal–organic frameworks with special topologies due to their rich coordination chemistry and the predictability of the resulting networks [4–6]. In addition, the aromatic polycarboxylates in conjunction with rare earth metals which possess high and variable coordination numbers and flexible coordination geometries, leading to the formation of the exotic molecular architectures.

Biphenyl-4,4′-dicarboxylic acid (H_2bpdc) shows several hallmarks: (1) structural characteristics of two carboxyl groups lying at two opposite sites lead to less space hindrance; (2) biphenyl groups may form rigid frameworks and larger cavities; (3) this ligand is highly reactive in aqueous solutions; (4) $bpdc^{2-}$ molecules interact actively with water molecules via hydrogen bonds [7, 8]. Therefore, the biphenyl-4,4′-dicarboxylic rigid, linear organic O-donor ligand is employed as organic linkers to construct metal–organic coordination compounds with a variety of coordination modes (Fig. 1) and different dimensionalities [8–19].

In our recent study on coordination polymers, a series of lanthanide(III) complexes using biphenyl-2,2′-dicarboxylic acid have been synthesized [20]. In this article, as a continuation of our previous work, we introduce the structural, thermal, and spectral investigations of lanthanide(III) coordination compounds based on another isomer of biphenyldicarboxylic ligand, namely biphenyl-4,4′-dicarboxylic acid. The principal aim of this study is the thermal research including the studies over thermal stability, pathway of decomposition process during heating under

J. Sienkiewicz-Gromiuk · Z. Rzączyńska (✉)
Department of General and Coordination Chemistry, Maria
Curie-Skłodowska University, M. C. Skłodowska Sq. 2, 20-031
Lublin, Poland
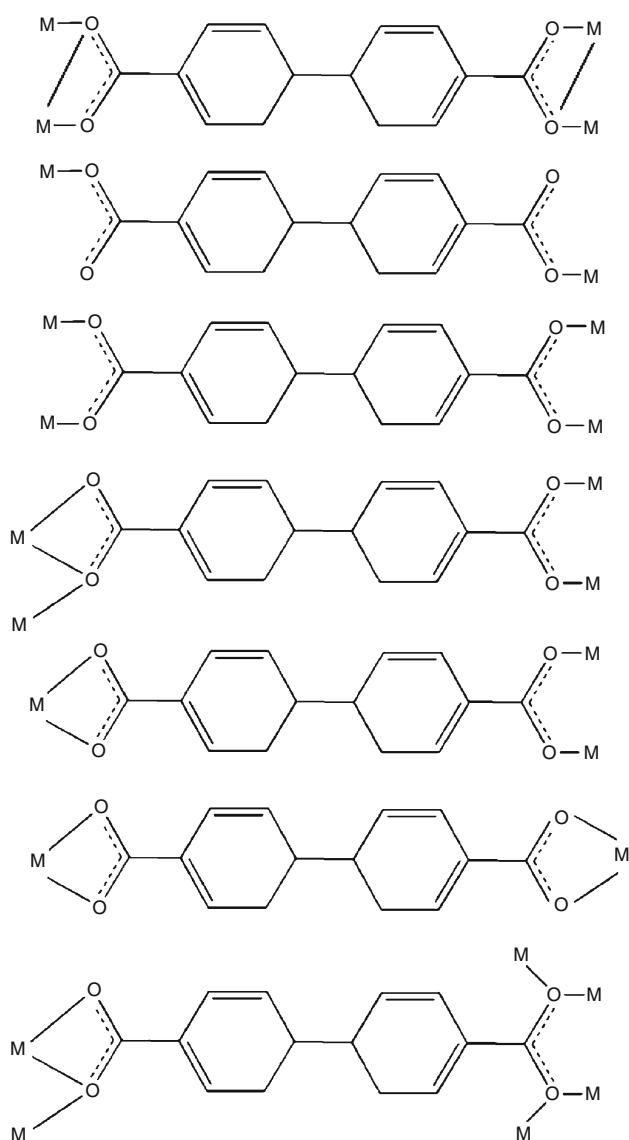e-mail: z.rzaczynska@poczta.umcs.lublin.pl

Fig. 1 Possible coordination modes of bpdc^{2-} ligand

several conditions (air and nitrogen atmosphere) and thermal effects related to these decomposition processes of analyzed compounds.

Experimental

Synthesis

The complexes of lanthanide(III) with biphenyl-4,4'-dicarboxylic acid were prepared by adding hot aqueous solutions of sodium biphenyl-4,4'-dicarboxylate (bpdc) dropwise (pH = 6.5) into the hot aqueous solution of rare earth chlorides (pH = 4.5–6.0) while stirring continuously. In the case of cerium(III), the nitrate solution was used. The precipitates were filtered, washed with hot water and dried at 30 °C to a

constant mass. All reagents were used in the commercial form. Lanthanide oxides (99.9 % purity) and biphenyl-4,4'-dicarboxylic acid (97 % purity) were produced by Aldrich.

Measurement methods

The contents of carbon and hydrogen were determined on the basis of elemental analyses by using a CHN 2400 Perkin Elmer instrument. The content of Ln^{3+} was established on the strength of thermogravimetric analyses (TG curves) using the oxalic method, which consists in calculating the metal contents from the obtained residues as the products of thermal decomposition of analyzed complexes. The results are presented in Table 1.

The complexes were identified on the basis of the FT-IR spectra recorded over the range 4,000–400 cm^{-1} in KBr disks using a FT-IR 1725X Perkin Elmer spectrometer.

All lanthanide compounds were also examined by the FT-Raman spectroscopy in the range 150–3,200 cm^{-1} using a Via Reflex Renishaw Raman spectrometer. The samples were irradiated using argon ionization ($\lambda = 514$ nm) or semiconductor ($\lambda = 785$ nm) laser with 10 min exposure time.

The thermal stability and decomposition of the prepared complexes in air were determined with the aid of Setsys 16/18, recording TG, differential scanning calorimetry (DSC), and DTG curves. The sample (7–8 mg) was heated in the Al$_2$O$_3$ crucible at 30–750 °C in flowing air atmosphere with a heating rate of 5 °C min^{-1}. The sample of La(III) and Lu(III) complexes was heated between 30 and 1,000 °C in dynamic air atmosphere with a heating rate 10 °C min^{-1}. Products of decomposition were calculated from the TG curves.

FT-IR spectra of gaseous products of thermal decomposition were registered on a Netzsch TG 209 instrument coupled to a Brucker FT-IR IFS66 spectrometer. The sample of gadolinium(III) and terbium(III) complexes was heated in dynamic argon atmosphere using a ceramic crucible and heating with a rate of 15 °C min^{-1} up to 1,000 °C.

The X-ray diffraction patterns were taken on a HZG-4 (Carl Zeiss, Jena) diffractometer ($2\theta = 3$–70° with a step equal to 0.05°) at ambient temperature. The XRAYAN program was used for determining positions and peak intensities. Pattern indexing was carried out with the PC version of TREOR program [21].

Results and discussion

Characterization and XRD studies

Bpdcs of lanthanide(III) were obtained as polycrystalline hydrates of typical color for Ln^{3+} ions. Based on the

Table 1 The elemental analysis data of bpdcs obtained under conventional conditions (bpdc = $C_{14}H_8O_4^{2-}$)

Complex	C/%		H/%		Ln/%	
	Found	Calc.	Found	Calc.	Found	Calc.
$La_2(bpdc)_3 \cdot 4H_2O$	46.95	47.08	2.96	2.99	26.02	25.95
$Ce_2(bpdc)_3 \cdot 4H_2O$	46.73	46.97	2.94	2.98	25.79	26.12
$Pr_2(bpdc)_3 \cdot 4H_2O$	47.44	46.91	2.93	2.98	26.01	26.67
$Nd_2(bpdc)_3 \cdot 5H_2O$	45.83	45.85	3.01	3.09	25.87	26.24
$Sm_2(bpdc)_3 \cdot 4H_2O$	45.82	46.09	2.90	2.93	28.49	27.50
$Eu_2(bpdc)_3 \cdot 4H_2O$	45.57	45.96	2.88	2.92	27.67	27.72
$Gd_2(bpdc)_3 \cdot 6H_2O$	44.38	44.09	3.11	3.15	27.42	27.51
$Tb_2(bpdc)_3 \cdot 6H_2O$	43.62	43.96	3.13	3.14	26.80	27.72
$Dy_2(bpdc)_3 \cdot 6H_2O$	43.31	43.69	3.07	3.12	28.35	28.17
$Ho_2(bpdc)_3 \cdot 6H_2O$	43.08	43.50	3.09	3.11	27.57	28.47
$Er_2(bpdc)_3 \cdot 5H_2O$	43.60	44.01	2.90	2.97	28.71	29.21
$Tm_2(bpdc)_3 \cdot 5H_2O$	43.72	43.88	2.91	2.96	29.10	29.42
$Yb_2(bpdc)_3 \cdot 4H_2O$	43.98	44.26	2.76	2.81	30.26	30.39
$Lu_2(bpdc)_3 \cdot 4H_2O$	44.04	44.11	2.75	2.80	31.34	30.63

analytical (Table 1) and TG data their formulae were defined as: $Ln_2(bpdc)_3 \cdot nH_2O$ where bpdc is the biphenyl-4,4'-dicarboxylate ligand $(C_{12}H_5(COO)_2^{2-})$; Ln is La–Lu and $n = 4$ for La–Pr, Sm, Eu, Yb and Lu; $n = 5$ for Nd, Er and Tm; $n = 6$ for Gd–Ho.

The X-ray diffraction patterns indicate that all lanthanide(III) bpdcs form crystalline powders. The majority of the investigated complexes crystallize in the triclinic crystal system (La–Dy, Tm and Yb), whereas the monoclinic cell parameters were ascribed to Ho, Er, and Lu compounds. The number of water molecules does not affect the crystal structures of the analyzed complexes (Table 2). In the series of lanthanide bpdcs three groups of isostructural complexes can be differentiated: (1) La(III)–Tb(III), (2) Dy(III) and Ho(III), (3) the complexes Er(III)–Lu(III). Figure 2 presents the X-ray pattern diffractions of neodymium(III), holmium(III), and lutetium(III) complexes as representatives of the above-mentioned isostructural series. As can be seen from the XRD patterns, the most intensive line is concurrently the first, regardless of the membership of concrete lanthanide ions to one of isostructural series. In the case of the XRD pattern of $Nd_2(bpdc)_3 \cdot 5H_2O$, the lowest number of sharp peaks is observed. This fact certainly indicates that the first series of isostructural complexes (La(III)–Tb(III)) forms complexes of lowest symmetry.

Table 2 The unit cell parameters for polycrystalline series of bpdcs (bpdc = $C_{14}H_8O_4^{2-}$)

| Complexes	Crystal system	a/Å	b/Å	c/Å	α/°	β/°	γ/°	Volume/Å^{-3}
$La_2(bpdc)_3 \cdot 4H_2O$	Triclinic	8.61	10.88	17.87	87.95	57.91	57.80	1127
$Ce_2(bpdc)_3 \cdot 4H_2O$	Triclinic	9.16	8.86	16.44	101.42	120.27	74.18	1105
$Pr_2(bpdc)_3 \cdot 4H_2O$	Triclinic	7.95	14.60	18.80	48.28	73.18	65.35	1479
$Nd_2(bpdc)_3 \cdot 5H_2O$	Triclinic	8.57	14.13	23.02	141.77	90.67	85.91	1715
$Sm_2(bpdc)_3 \cdot 4H_2O$	Triclinic	6.57	13.17	17.16	122.31	78.26	91.18	1223
$Eu_2(bpdc)_3 \cdot 4H_2O$	Triclinic	7.84	14.29	16.06	114.16	115.65	57.66	1332
$Gd_2(bpdc)_3 \cdot 6H_2O$	Triclinic	12.41	11.86	19.68	53.77	49.54	53.81	1674
$Tb_2(bpdc)_3 \cdot 6H_2O$	Triclinic	9.63	13.27	18.01	128.84	108.98	55.32	1472
$Dy_2(bpdc)_3 \cdot 6H_2O$	Triclinic	7.40	14.90	15.92	79.10	83.15	106.40	1626
$Ho_2(bpdc)_3 \cdot 6H_2O$	Monoclinic	14.00	13.39	9.58	90.00	96.82	90.00	1782
$Er_2(bpdc)_3 \cdot 5H_2O$	Monoclinic	15.21	6.17	14.45	90.00	101.30	90.00	1330
$Tm_2(bpdc)_3 \cdot 5H_2O$	Triclinic	9.30	13.60	14.80	78.09	78.38	67.65	1678
$Yb_2(bpdc)_3 \cdot 4H_2O$	Triclinic	8.76	16.19	15.29	78.96	79.96	63.77	1900
$Lu_2(bpdc)_3 \cdot 4H_2O$	Monoclinic	17.18	7.57	15.82	90.00	115.27	90.00	1860
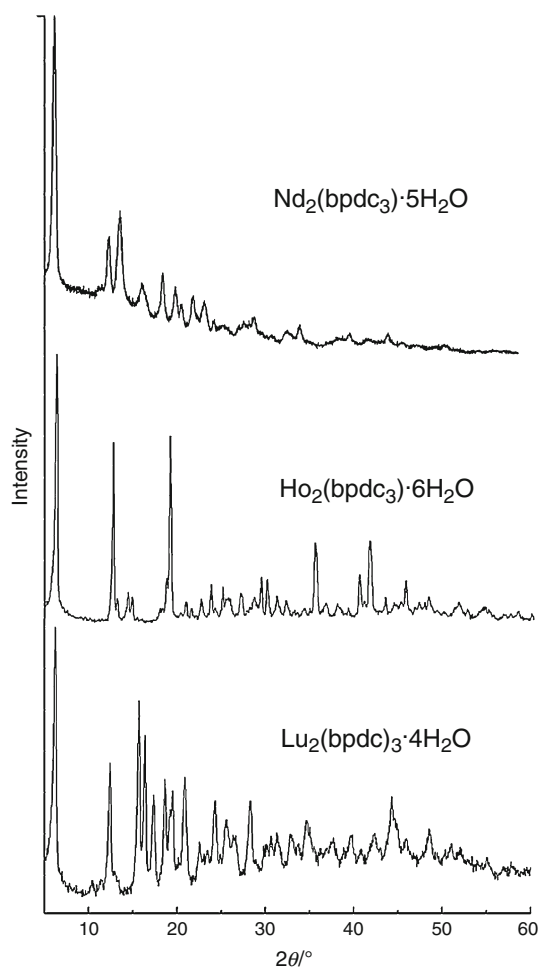
Fig. 2 X-ray diffraction patterns of representatives of isostructural series of lanthanide biphenyl-4,4′-dicarboxylates

FT-IR and FT-Raman investigations

All investigated lanthanide(III) bpdcs were characterized by FT-IR and FT-Raman spectroscopy exhibiting similar solid state spectra. The experimental FT-IR and FT-Raman spectra of free H_2bpdc ligand and its lanthanum(III), terbium(III), and lutetium(III) complexes are presented in Figs. 3 and 4. The symbols used denote the following: v stands for the stretching vibrations; β for the in-plane deformation modes; γ for the out-of-plane bending modes, and Ar for aromatic carbon atoms vibrations. Replacement of the carboxylic groups' hydrogen with a metal ion brings about some characteristic changes in the FT-IR and FT-Raman spectra of the metal complexes in comparison with those of free ligand. The most important change observed between the FT-IR spectra of acid and its salts is appearance of the asymmetric and symmetric stretching vibrations of carboxylate anion $v_{as}(COO^-)$ and $v_s(COO^-)$ in the spectra of lanthanide(III) complexes in the regions 1,580–1,576 and 1,441–1,402 cm^{-1}, respectively, instead of very diagnostic
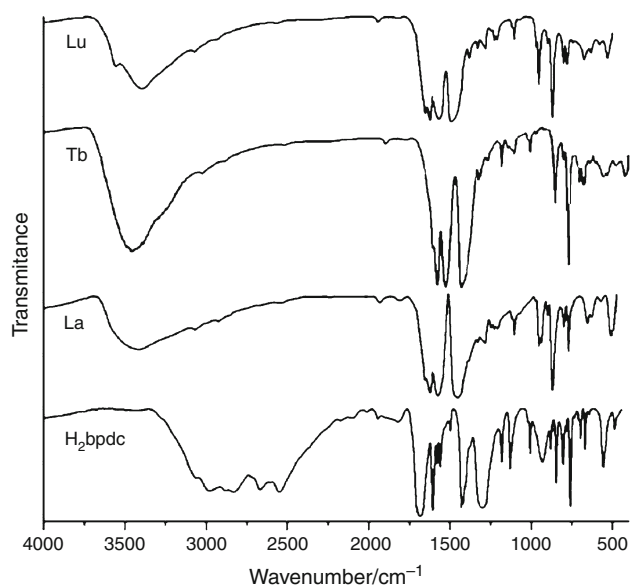

Fig. 3 Experimental FT-IR spectra of H_2bpdc ligand and its La(III), Tb(III), and Lu(III) complexes
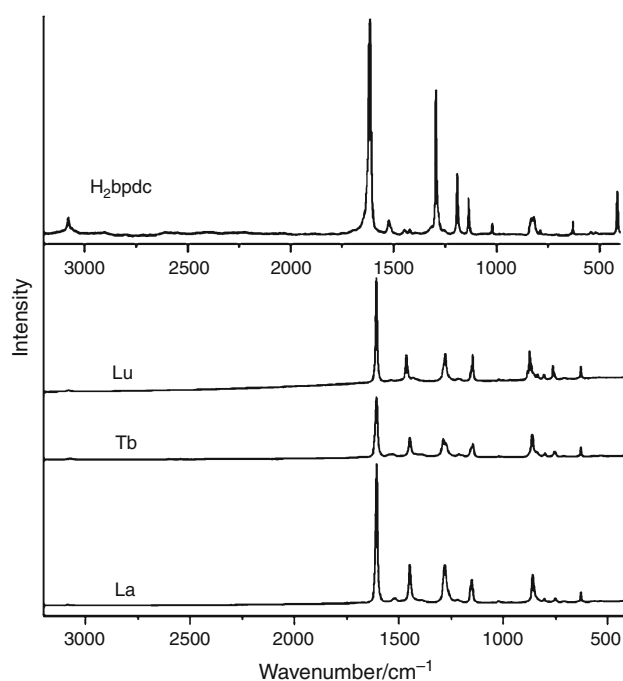

Fig. 4 Experimental FT-Raman spectra of H_2bpdc ligand and its La(III), Tb(III), and Lu(III) complexes

absorption bands derived from the stretching $v(C=O)$ vibrations of carboxylic groups at 1,684 cm^{-1} observed in the FT-IR spectra of free ligand. Appearance of these absorption bands of $-COO^-$ groups proves that bpdc ligand is successfully coordinated by lanthanide ions in the studied complexes. Other significant changes connected with transformation of carboxylic groups into carboxylate anions are the absence of the other absorption bands which derived

from the nonionized carboxylic groups of free acid at 1427 [v(C–O)], 1295 [β(COH)], and 931 cm^{-1} [γ(COH)] confirm the complete deprotonation of acid. The presence of water molecules in the structures of the investigated complexes was confirmed by the broad absorbance band in the range 3,700–2,500 cm^{-1} characteristic of stretching vibrations of hydroxyl groups v(OH) of hydrogen-bonded water molecules. The bands due to the metal–oxygen bond appear at 431–411 cm^{-1} for the whole series of complexes. Putting the metal ions into the structure of free ligand induces the differences in the density charge distribution in the new-formed metal–ligand structure of complexes, which consequently also brings the insignificant changes connected with disappearance and shifting of the position of some typical aromatic bands derived from the biphenyl group, despite the fact that biphenyl system does not take part in the coordination process. Thus, the FT-Raman spectra of lanthanide(III) complexes were recorded and collated with the FT-IR spectra to make sure that faultless assignments of the individual absorption bands to suitable vibrations come from nonpolar atom groups, like aromatic carbon–carbon and carbon–hydrogen vibrations.

Thermal analysis (TG–DSC) in air

To investigate thermal stability and decomposition of the complexes under investigation, the TG analysis and the DSC were performed for the crystalline samples. All lanthanide(III) bpdcs are stable at ambient temperature but further heating leads to gradual decomposition (Fig. 5; Table 3). The thermal decomposition of hydrated investigated compounds in air proceeds in two principal stages, including dehydration process and degradation of anhydrous form of studied complexes. The first significant weight loss observed on the TG curves (Fig. 5) corresponds to the removal of water molecules from the structure of hydrated complexes. The dehydration enthalpies found for bpdcs were in the range 83–306 kJ mol^{-1}.

In the case of the complexes from cerium(III) to europium(III), ytterbium(III) and lutetium(III), heating over 30 °C initiates the one-step dehydration process, which takes place up to 150–220 °C. The TG curves in the aforementioned temperature range show loss of mass by about 6.57–7.24 %, which corresponds to the loss of four water molecules, whereas the TG profile of neodymium(III)

Fig. 5 TG and DSC *curves* of thermal decomposition in air atmosphere of La$_2$(bpdc)$_3$·4H$_2$O (**a**), Nd$_2$(bpdc)$_3$·5H$_2$O (**c**), and Lu$_2$(bpdc)$_3$·4H$_2$O (**e**) down to augmentation of the range of dehydration process of above-mentioned La (**b**), Nd (**d**) and Lu (**f**) complexes
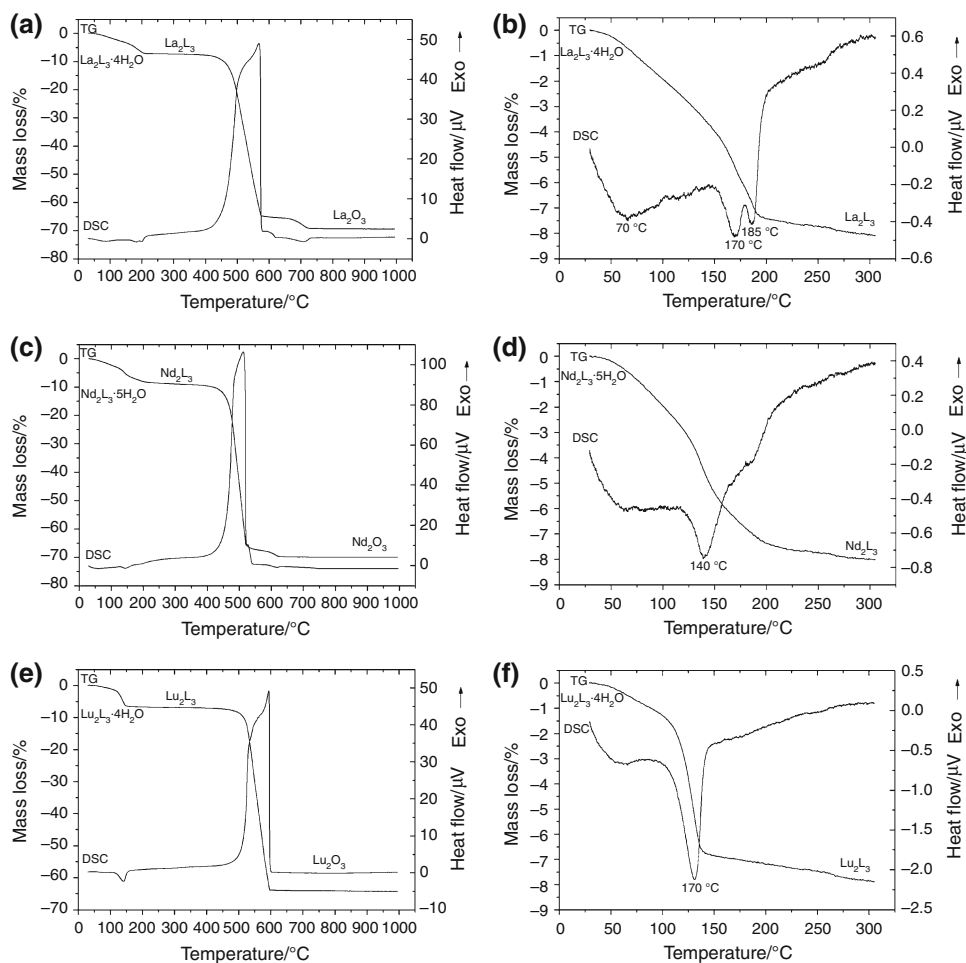
Table 3 Thermoanalytical data of lanthanide(III) bpdcs (air); L = $(C_{14}H_8O_4)^{2-}$

Complex	ΔT_1/°C	Mass loss/%		Endothermic effect/J g^{-1}	ΔT_2/°C	Total mass loss/%		Final product
		Calc.	Found			Calc.	Found	
$La_2L_3 \cdot 4H_2O$	30–220	6.73	7.15	106	395–740	69.56	69.49	La_2O_3
$Ce_2L_3 \cdot 4H_2O$	30–200	6.71	7.19	83	310–440	67.92	68.14	CeO_2
$Pr_2L_3 \cdot 4H_2O$	30–205	6.70	7.24	164	405–555	68.31	68.58	Pr_6O_{11}
$Nd_2L_3 \cdot 5H_2O$	30–220	8.19	8.39	185	395–640	69.39	69.67	Nd_2O_3
$Sm_2L_3 \cdot 4H_2O$	30–200	6.59	6.94	173	400–610	68.11	67.79	Sm_2O_3
$Eu_2L_3 \cdot 4H_2O$	30–200	6.57	6.83	227	350–625	67.91	67.97	Eu_2O_3
$Gd_2L_3 \cdot 6H_2O$	30–80	3.15	3.02	306	405–630	68.29	68.39	Gd_2O_3
$Gd_2L_3 \cdot 4H_2O$	80–200	6.30	6.11					
$Tb_2L_3 \cdot 6H_2O$	30–90	3.14	2.86	152	410–540	67.39	67.68	Tb_4O_7
$Tb_2L_3 \cdot 4H_2O$	90–160	6.28	6.38					
$Dy_2L_3 \cdot 6H_2O$	30–85	3.12	3.20	285	440–560	67.67	67.48	Dy_2O_3
$Dy_2L_3 \cdot 4H_2O$	85–145	6.24	5.94					
$Ho_2L_3 \cdot 6H_2O$	30–85	3.11	3.23	260	440–565	67.39	67.62	Ho_2O_3
$Ho_2L_3 \cdot 4H_2O$	85–155	6.22	6.23					
$Er_2L_3 \cdot 5H_2O$	30–110	4.72	4.95	167	435–555	66.60	66.40	Er_2O_3
$Er_2L_3 \cdot 2H_2O$	110–150	3.14	3.01					
$Tm_2L_3 \cdot 5H_2O$	30–100	3.14	2.92	121	450–560	66.40	66.24	Tm_2O_3
$Tm_2L_3 \cdot 3H_2O$	100–155	4.70	4.67					
$Yb_2L_3 \cdot 4H_2O$	30–150	6.32	6.74	111	440–550	65.39	65.54	Yb_2O_3
$Lu_2L_3 \cdot 4H_2O$	30–170	6.30	6.57	124	440–605	65.17	65.43	Lu_2O_3

ΔT_1, temperature range of dehydration process; ΔT_2, temperature range of decomposition of anhydrous complexes to oxides

compound demonstrates the weight loss of 8.39 %, which is associated with elimination of five water molecules. Although, only one obvious weight loss is observed, the shape of peaks on the DSC curves indicates that water molecules are released in the overlapping stages. The evident mass loss is accompanied by the endothermic effect with the peak top at 110 °C (for Nd and Eu), 115 °C (for Sm), 130 °C (for Yb and Lu), 140 °C (for Pr), and 150 °C (for Ce) (Fig. 5).

The dehydration process in bpdcs from gadolinium(III) to thulium(III) hydrates proceeds in two steps and represents the loss of two and remaining (four or three) water molecules, respectively. In comparison with one-stage dehydration, the dehydration process for hexa- and pentahydrates in question also begins at 30 °C and runs to the relatively lower temperature range 150–160 °C (except $Gd_2(bpdc)_3 \cdot 6H_2O$, where dehydration increases up to 200 °C). The first dehydration step observed on the TG curves is characterized by the weight loss in the range 2.86–4.95 %. These mass losses are related to the endothermic effect (observed on the DSC curves) with the maxima at 70 °C (Gd(III) and Dy(III) complexes), 75 °C (Tb(III), and Ho(III) compounds), 85 °C (Tm(III) complex) and 95 °C (Er(III) compound). The remaining water molecules (four or three) are evolved in the temperature range 85–160 °C (Table 3). The maxima of endothermic

effects attributed to the second step of dehydration process appear at 105 °C (Gd(III), Dy(III) and, Ho(III) complexes), 115 °C (Tb(III) compound) and 130 °C (Er(III) and Tm(III) complexes) (Fig. 5).

Removal of water molecules in the $La_2bpdc_3 \cdot 4H_2O$ complex proceeds in a more complicated way. The TG curve shows only one appreciable dehydration step, while DSC profile shows not clearly separated three endothermic peak tops at 70, 170, and 185 °C which permit us to presume stepwise dehydration (Fig. 5a, b).

After the complete removal of water molecules from the hydrated complexes the anhydrous compounds (Ln_2bpdc_3) are formed. The TG curves show plateau up to 310–450 °C which indicates a wide range of stability of anhydrous compounds. On further heating, the anhydrous compounds decompose directly to suitable oxides (CeO_2, Pr_6O_{11}, Tb_4O_7, and $Ln(Dy–Lu)_2O_3$). The temperature range of beginning of oxides formation is about 540–605 °C. The temperature of establishing of CeO_2 is much lower and it reaches approximately 440 °C. In the case of the La(III) complex and compounds from Nd(III) to Gd(III) the corresponding oxides are formed by various intermediate forms. The temperature of oxides formation is higher than that of direct oxide formation and changes from 610 °C for Sm_2O_3, to 740 °C for La_2O_3. The DSC curve indicates that the decomposition of organic ligand is connected with a

very strong exothermic effect with the peak top near 500 °C (490–540 °C). In the case of cerium(III) and europium(III) complexes, the exothermic peak tops occur at 400 and 425 °C, respectively (Table 3).

TG–FT-IR analysis in argon

The simultaneous TG analysis in argon coupled with the FT-IR spectroscopy was performed for the crystalline sample of $Tb_2bpdc_3 \cdot 6H_2O$ as a complement to the thermal analysis obtained in air. This measurement technique enables determination of the way of complexes decomposition in atmosphere without oxygen and identification of the emitted gaseous products, which evolved during their thermal degradation. The mode of thermal decomposition of the analyzed complex in argon and in air atmosphere in the whole temperature range is similar (Fig. 6). As follows from Fig. 6, one noticeable difference, found on the thermal graphs obtained in argon, is the temperature of beginning of degradation of the organic ligand, which is shifted toward higher temperature by 100 °C (510 °C), compared to the thermal analysis performed in air. From the obtained results, it can be stated with type of flowing gases does not affect the pathway of the dehydration process, the increasing thermal stability of the anhydrous form of the studied complexes. The line plot of the FT-IR spectra of the leaked gases for $Tb_2bpdc_3 \cdot 6H_2O$ are given

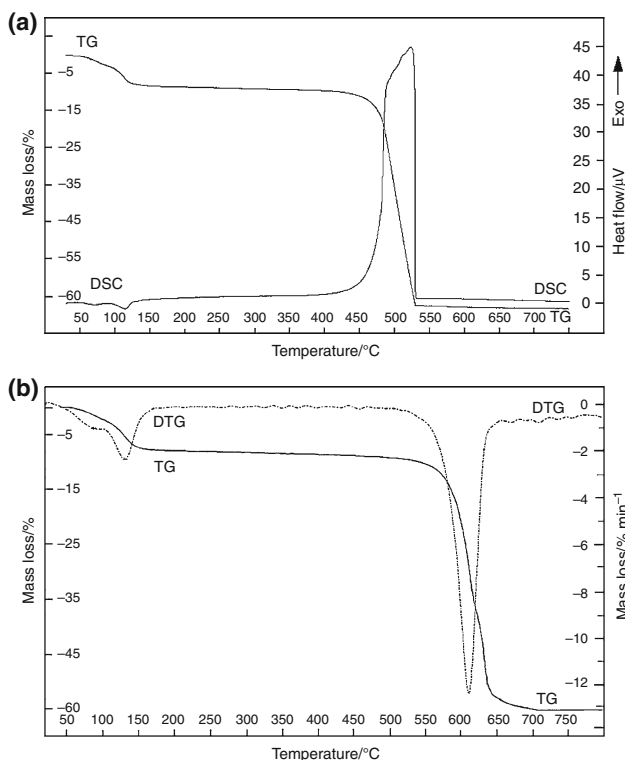**Fig. 6** TG, DSC and DTG *curves* of decomposition process of $Tb_2(bpdc)_3 \cdot 6H_2O$ in air (**a**) and in argon (**b**) atmosphere
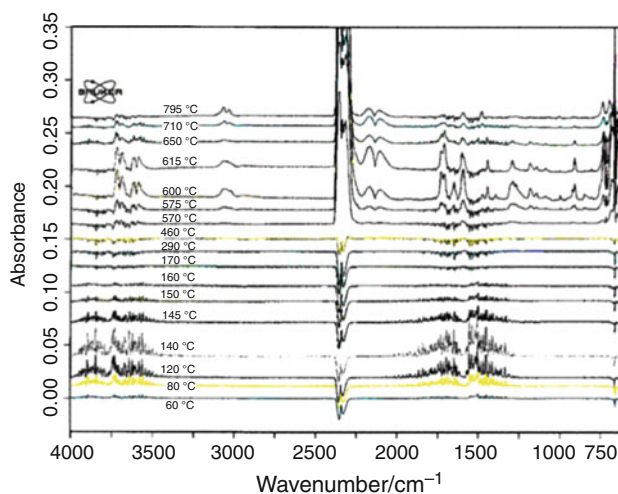

Fig. 7 *Line plot* of FT-IR spectra of the evolved gases for $Tb_2(C_{14}H_8O_4)_3 \cdot 6H_2O$

in Fig. 7. The FT-IR spectra recorded in the range of 50–170 °C show the absorption bands in the wavenumbers: 4,000–3,500 and 1,900–1,300 cm^{-1} attributed to the stretching and deformation vibrations of hydroxyl groups $v(O–H)$ from water molecules. Further heating up to about 510 °C does not cause release of any gaseous products that is characteristic of formation of stable anhydrous complex. Over this temperature, characteristic double bands of absorbed CO_2 molecules at 2365, 2315 cm^{-1} and those in the range 750–600 cm^{-1} are observed due to the degradation of Tb_2bpdc_3 compound. At a higher temperature (575 °C), the molecules of carbon monoxide are released and their characteristic double-band with the maxima at 2160, 2105 cm^{-1} are detected. Around 600 °C the weak absorption bands at 3080, 3040, and 1300–850 cm^{-1} corresponding to the stretching and deformation vibrations of $v(C–H)$ groups come from hydrocarbons [22–27].

Conclusions

In conclusion, a hydrated polycrystalline series of lanthanide complexes with biphenyl-4,4′-dicarboxylic acid was synthesized by means of the conventional precipitation method. The powder X-ray analysis revealed that they belong to three isostructural groups. The complexes are stable at room temperature, but heating causes one or two steps release of water molecules. After removal of all solvent molecules, the stable intermediate compounds Ln_2bpdc_3 are formed. The anhydrous complexes decompose directly or through intermediate forms to corresponding oxides. The modes of decomposition have been confirmed by the TG–FT-IR study and schematically proceed as follows:

- tetrahydrated complexes:

  (a) $Ln_2bpdc_3\cdot 4H_2O \rightarrow Ln_2bpdc_3 \rightarrow Ln_2O_3$, where $Ln = La, Sm, Eu, Yb, Lu; Ce_2bpdc_3\cdot 4H_2O \rightarrow Ce_2bpdc_3 \rightarrow 2CeO_2; \quad 3[Pr_2bpdc_3\cdot 4H_2O] \rightarrow 3Pr_2bpdc_3 \rightarrow Pr_6O_{11}$;

- pentahydrated complexes:

  (a) $Nd_2bpdc_3\cdot 5H_2O \rightarrow Nd_2bpdc_3 \rightarrow Nd_2O_3$;
  (b) $Er_2bpdc_3\cdot 5H_2O \rightarrow Er_2bpdc_3\cdot 2H_2O \rightarrow Er_2bpdc_3 \rightarrow Er_2O_3$;
  (c) $Tm_2bpdc_3\cdot 5H_2O \rightarrow Tm_2bpdc_3\cdot 3H_2O \rightarrow Tm_2bpdc_3 \rightarrow Tm_2O_3$;

- hexahydrated compound:

  (a) $Ln_2bpdc_3\cdot 6H_2O \rightarrow Ln_2bpdc_3\cdot 4H_2O \rightarrow Ln_2bpc_3 \rightarrow Ln_2O_3$, where $Ln = Gd, Dy, Ho; 2[Tb_2bpdc_3\cdot 6H_2O] \rightarrow 2[Tb_2bpdc_3\cdot 4H_2O] \rightarrow 2Tb_2bpdc_3 \rightarrow Tb_4O_7$.

References

1. Kitagawa S, Matsuda R. Chemistry of coordination space of porous coordination polymers. Coord Chem Rev. 2007;251: 2490–509.
2. Yaghi OM, O'Keeffe M, Ockwig NW, Chae HK, Eddaoudi M, Kim J. Reticular synthesis and the design of new materials. Nature. 2003;423:705–14.
3. Neofotistou E, Malliakas CD, Trikalitis PN. Unprecedented sulfone-functionalized metal–organic frameworks and gas-sorption properties. Chem Eur J. 2009;15:4523–7.
4. Wang SN, Xing H, Li YZ, Bai J, Pan Y, Scheer M, You XZ. 2D and 3D cadmium(II) coordination polymers from a flexible tripodal ligand of 1,3,5-tris(carboxymethoxy)benzene and bidentate pyridyl-containing ligands with three-, eight- and ten-connected topologies. Eur J Inorg Chem. 2006;3041–53.
5. Lan YQ, Wang XL, Li SL, Su ZM, Shao KZ, Wang EB. An unprecedented (6,8)-connected self-penetrating network based on two distinct zinc clusters. Chem Commun. 2007;4863–5.
6. Wang XL, Qin C, Wang EB, Su ZM, Xu L, Batten SR. An unprecedented eight-connected self-penetrating network based on pentanuclear zinc cluster building blocks. Chem Commun. 2005; 4789–91.
7. Han YF, Zhou XH, Zheng YX, Shen Z, Song Y, You XZ. Syntheses, structures, photoluminescence, and magnetic properties of nanoporous 3D lanthanide coordination polymers with 4,4′-biphenyldicarboxylate ligand. CrystEngComm. 2008;10:1237–42.
8. Pan L, Ching N, Huang X, Li J. Reactions and reactivity of Co–bpdc coordination polymers (bpdc = 4,4′-biphenyldicarboxylate). Inorg Chem. 2000;39:5333–40.
9. Wang YB, Zhuang WJ, Jin LP, Lu SZ. Solvothermal synthesis and structures of lanthanide-organic sandwich coordination polymers with 4,4′-biphenyldicarboxylic acid. J Mol Struct. 2004;705:21–7.
10. Hu R, Cai H, Luo J. Synthesis, structure and luminescent property of a pillared-layer coordination polymer [Pb(BPDC)] (BPDC = 4,4′-biphenyldicarboxylate). Inorg Chem Commun. 2011;14:433–6.
11. Yu B, Wang XQ, Kou HZ, Shen GQ, Shen DZ. Poly[[diaquasamarium(III)]-μ_3-(biphenyl-4,4′-dicarboxylato)-μ_3-(4′-carboxylbiphenyl-4-carboxylato)]. Acta Crystallogr. 2006;E62:m3078–9.
12. Guo X, Zhu G, Fang Q, Xue M, Tian G, Sun J, Li X, Qiu S. Synthesis, structure and luminescent properties of rare earth coordination polymers constructed from paddle-wheel building blocks. Inorg Chem. 2005;44:3850–5.
13. Yuen T, Lin CL, Zan JA, Pan L, Li J. Magnetic properties of a metal–organic chain system [Co(bpdc)(H$_2$O)$_2$]·H$_2$O (bpdc = biphenyldicarboxylate). J Appl Phys. 2005;97:10B315-1–3.
14. Long LS, Ren YP, Ma LH, Jiang YB, Huang RB, Zheng LS. A unique three-dimensional coordination polymer constructed from 4,4′-biphenyldicarboxylate and zinc(II). Inorg Chem Commun. 2003;6:690–3.
15. Liang Y, Hong M, Cao R, Weng J, Su W. Hydrothermal synthesis and characterization of the coordination polymer [Zn(bbdc)(H$_2$O)]$_n$ (bbdc = 4,4′-bibenzene-dicarboxylate) possessing a 3D network structure. Inorg Chem Commun. 2001;4:599–601.
16. Kongshaug KO, Fjellvåg H. Organically pillared layered zinc hydroxides. J Solid State Chem. 2004;177:1852–7.
17. Zheng PQ, Long LS, Huang RB, Zheng LS. Crystal structure of a 3D coordination polymer: [Cd(BPDC)(H$_2$O)]$_n$ (BPDC = 4,4′-biphenyldicarboxylate). Main Group Met Chem. 2002;25: 701–2.
18. He J, Zhang Y, Yu J, Pan Q, Xu R. Two 2-D 3^6 tessellated metal–organic frameworks constructed from trimetallic clusters and dicarboxylate ditopic links. Mater Res Bull. 2006;41:925–33.
19. Pan L, Finkel BS, Huang X, Li J. The first pillared three-dimensional structure constructed by carboxylate ligands bridging heterometallic trilayers. Chem Commun. 2001;105–6.
20. Rzączyńska Z, Sienkiewicz-Gromiuk J, Głuchowska H. Structural and thermal properties of rare earth complexes with 2,2′-biphenyldicarboxylic acid. J Therm Anal Calorim. 2010;101: 213–9.
21. Werner PE. TREOR—trial and error program for indexing of unknown powder patterns. Stockholm: University of Stockholm; 1984.
22. Łyszczek R. Comparison of thermal properties of lanthanide trimellitates prepared by different methods. J Therm Anal Calorim. 2008;93:833–8.
23. Silverstein R, Webster FX. Spectrometric identification of organic compounds. New York: Wiley; 1998.
24. Socrates G. Infrared and Raman characteristic group frequencies: tables and charts. Chichester: Wiley; 2001.
25. Łyszczek R. Hydrothermal synthesis, thermal and luminescent investigations of lanthanide(III) coordination polymers based on the 4,4′-oxybis(benzoate) ligand. J Therm Anal Calorim. 2012; 108:1101–10.
26. Teixeira KC, Moreira GF, Quirino WG, Legnani C, Silva RA, Cremona M, Brito HF, Achete CA. Rare-earth based OLEDs TG-FTIR thermal stability investigation of tetrakis beta-diketonates complexes. J Therm Anal Calorim. 2011;106:587–93.
27. Czylkowska A, Markiewicz M. Synthesis, thermal behavior, and other properties of Y(III) and La(III) complexes with 4,4′-bipyridine and trichloro- or dibromoacetates. J Therm Anal Calorim. 2012. doi:10.1007/s10973-012-2454-8.